In: *Hazardous Seas: A sociotechnical framework for early tsunami detection and warning*, ed. by L.K. Comfort and H.P. Rahayu, Island Press, pp. 221–245, 2023.

Chapter 9

A Prototype Ocean Bottom Pressure Sensor Deployed in the Mentawai Channel, Central Sumatra, Indonesia: Preliminary Results

Emile A. Okal and Lee Freitag

In this chapter, we analyze data retrieved from an ocean floor pressure sensor continuously operated for forty-eight days in Indonesia's Mentawai Channel during the spring of 2016 as part of Project Hazard SEES, Interdisciplinary Research in Hazards and Disasters, funded by the US National Science Foundation. Initial processing through systematic spectrogram analysis has identified eight distant earthquakes recorded through the variation of pressure accompanying the passage of seismic waves on the bottom of the ocean. The analysis of the corresponding wave trains allows the recovery of the standard magnitude M_S of five of the events (two more being intermediate depth and the eighth antipodal) with a residual not exceeding 0.2 logarithmic unit. We also show that the classical energy-to-moment ratio computation can be successfully adapted by defining a response function of the pressure sensor to teleseismic *P* waves. In addition, six local earthquakes, occurring at distances of 58 to 670 kilometers from the sensor, but with magnitudes less than 5.5, were also recorded. We show that an estimate of the seismic energy radiated by these events can be obtained from a simple integration of the square of the pressure signal. Thus, our results indicate that meaningful quantitative estimates of the source characteristics of both teleseismic and regional events can be obtained through robust methods based on single-station pressure recordings on the ocean floor.

This chapter is adapted from L. Freitag and E. A. Okal, 2020, "Preliminary results from a prototype ocean-bottom pressure sensor deployed in the Mentawai Channel, Central Sumatra, Indonesia," *Pure and Applied Geophysics* 177: 5119–31, https://doi.org/10.1007/s00024-020-02561-6.

Background and Motivation: A Layman's Discussion of the Science behind Seismic Tsunami Warning

This chapter reports on the experimental operation of a prototype ocean bottom pressure sensor in the context of tsunami detection in the Mentawai Channel between Siberut Island and the large island of Sumatra, Indonesia, to the northeast (see the map in the preface).

Sumatra, at the western extremity of Indonesia, borders a so-called subduction zone where the Australian tectonic plate sinks underneath the Eurasian one. This sinking process is taking place principally through large earthquakes, some of them generating catastrophic tsunamis, most recently during the 2004 Sumatra-Andaman event (Synolakis et al. 2005).

Our field location, off the central part of Sumatra, was the site of megaearthquakes in 1797 (northern half) and 1833 (southern half) (Zachariasen et al. 1999; Natawidjdaja et al. 2006). To the south, part of the 1833 fault zone ruptured again during the 2007 Bengkulu earthquake (Borrero et al. 2009), thus releasing at least part of the tectonic stress accumulated over 175 years. By contrast, in the vicinity of Siberut, the plate interface is believed to be locked in the form of a so-called seismic gap, where conditions are now believed ripe for a "megathrust" event to take place in the next years or decades. Such an earthquake would probably generate a tsunami with potentially catastrophic consequences for Padang, a nearby port city with a 2019 metropolitan population of 1.4 million (Borrero et al. 2006).

Tsunami warning rests fundamentally on the detection of the parent earthquake and its real-time interpretation in terms of potential for tsunami generation. In very general terms, all seismic waves can be satisfactorily modeled by representing their source as an appropriate combination of forces (known as a moment tensor) and applying the principles of mechanics to Earth considered as an elastic body. That framework has been extended to the modeling of tsunamis, which can be considered as a particular case of the large family of seismic waves; in simple terms, the mechanical process that excites the waves is the same one that generates the tsunami.

Because of the linearity of the equations of motion, both in elasticity theory and to a large extent in fluid mechanics, one would expect the amplitudes of seismic waves and tsunamis to be scaled and thus for the former to be appropriate predictors of the latter. Such scaling is at the core of tsunami warning. Once the "size" of the earthquake is known, its tsunami potential should be predictable. In this context, and in the

near field where warning efforts do not have the luxury of time, a simple message from the scientific community to the populations at risk has consistently been "*the shaking is the warning*," that is, if you feel it and you are close to the shoreline, waste no time and self-evacuate to a safe height, typically 10 meters or more.

In scientific terms, the size of the earthquake has been described since the works of Vvedenskaya (1956) in Russia and Knopoff and Gilbert (1959) in the United States as a bona fide physical measurement, known as the seismic moment M_0 of the system of forces mentioned above, measured in physical units of dynes times centimeters (dyn * cm) or newtons times meters (N * m). Aki (1966) and later Dziewonski et al. (1981) have formalized methodologies for the routine measurements of M_0, now available from worldwide observations within 10 to 20 minutes following an earthquake (Kanamori and Rivera 2008). Kanamori (1977) has derived a protocol to represent M_0 as a so-called moment magnitude M_w designed to be comparable to estimates of conventional magnitudes developed, notably by Richter (1935) and later Gutenberg (1945), at a time when theoretical seismology lacked adequate bases for the representation of seismic sources as moment tensors, but were still widely used in observational seismology and by the media.

In lay terms, the concept of scaling of seismic sources assumes that all their properties (such as seismic slip on the fault plane, length of rupture, areas of given felt intensities, and duration of slip at the source) grow in unison and can be predicted from a single number, namely the seismic moment M_0 or its magnitude rendition M_w. Remarkably, this conjecture has been verified overwhelmingly not only among major earthquakes, but also during minor cracks induced by activity such as mining or fracking and also in laboratory studies on single crystals, across a total of seventeen orders of magnitude for M_0 (Ide and Beroza 2001).

Unfortunately, although most earthquakes are well-behaved and do follow scaling laws, seismological practice has identified in the past few decades a number of anomalous events in clear violation of the paradigm. In very simple terms, one can think of the set of seismic waves generated during an earthquake as a kind of Earth symphony; in most cases, it is perfectly balanced, but some maverick events will emphasize the bass (in spectroscopic terms, they would be called "red-shifted"), while others may favor the trebles (and as such would be "blue-shifted"). In short, for such rogue earthquakes, a single value of seismic moment or moment magnitude may not tell the whole story about their seismic source.[1]

Because tsunamis have periods typically ranging from tens of minutes

to 1 hour, their generation is controlled by the lowest-frequency part of the seismic source spectrum, while waves responsible for shaking felt by individuals have typical periods of 1 second or less. In this context, it is clear that anomalous earthquakes featuring an uneven spectrum will violate the expected relationship between the two effects and as such constitute a serious challenge for tsunami warning.

The class of red-shifted, *slow* earthquakes is particularly treacherous, a classic example being the 1992 Nicaraguan tsunami. Its "body-wave" magnitude, measured at a period of 1 second, $m_b = 5.3$, was so low that the earthquake was felt only weakly along certain sections of the shore and even not at all in others. Its source, however, was hiding its full size at longer periods, typically 300 seconds and longer, with a moment magnitude reaching $M_w = 7.6$. The result was a powerful tsunami that reached 10 meters in run-up (defined as the maximum altitude of land inundated by a tsunami) and killed 170 people, eradicating several villages where the earthquake had not been felt (Abe et al. 1993). In such instances, the simple adage "*the shaking is the warning*" cannot apply. In a classic paper based on similar events in 1896 in Sanriku, Japan, and in 1946 in the Aleutian Islands, Kanamori (1972) had coined the name "tsunami earthquakes" for the class of such earthquakes whose tsunamis are much larger than would be predicted by their seismic waves, especially at periods conventionally associated with felt effects.

By contrast, a number of earthquake sources have been found to be "blue-shifted," that is, to have a spectrum enriched in high frequencies, leading to enhanced destruction and casualties through excessive ground accelerations. One such acceleration reached in excess of 20 meters per second squared, or more than twice Earth's gravity, during the 2011 Christchurch, New Zealand, earthquake (Kaiser et al. 2012), an otherwise moderate event ($M_w = 6.2$). Because these sources correspond to a source with a faster than expected stress release, they can be referred to as "brisk" or "snappy."

Motivated by the occurrence of three tsunami earthquakes in Nicaragua in 1992, Java in 1994, and northern Peru in 1996, researchers led a considerable effort to understand the processes leading to departure from scaling laws in the years and decades following these events (Choy and Boatwright 1995; Tanioka et al. 1997; Polet and Kanamori 2000). In particular, Newman and Okal (1998) introduced a slowness parameter Θ, allowing to quantify the anomalous character of an earthquake. Because it requires an estimate of the seismic moment, however, the parameter Θ is generally not immediately available in real time for the benefit of

tsunami warning in the near field. In this context, later work by Convers and Newman (2013) and Okal (2013) has focused on exploiting the duration of high-frequency seismic waves as evidence of earthquake slowness.

One of the most fundamental questions regarding tsunami earthquakes is whether they feature a regional component, that is, whether they tend to occur in specific regions or rather could happen along any subduction zone. Many studies, including of historical events predating the development of modern, digital seismic instrumentation, have identified a catalog of more than twenty tsunami earthquakes with documented cases as early as 1896, 1907, and 1923 (Martin et al. 2019, table 6). In this context, preliminary evidence would suggest that many, and probably all, subduction zones can entertain tsunami earthquakes, notably in the form of aftershocks of regular megathrust events (e.g., Fukao 1979; Okal and Borrero 2011; Salaree and Okal 2018).

The departure of seismic sources from the canons of scaling laws took a particularly dramatic turn during the 2009–2010 sequence of events in and around our field area. On September 30, 2009, a catastrophic earthquake hit the city of Padang, causing considerable damage and upwards of eleven hundred deaths (Bothara et al. 2010). However, it generated only a minor tsunami with a maximum run-up of 27 centimeters, due to the earthquake's location at a depth of 80 kilometers, inside the subducting slab rather than at the plate interface, thus offsetting most of the rupture area under Sumatra (in simple terms, the earthquake moved more rock than water). In addition, the 2009 Padang earthquake was clearly of a "snappy," blue-shifted character, with its source not exceeding 10 seconds in duration, later confirmed through a high energy-to-moment parameter Θ (Saloor and Okal 2018). This situation falsely instilled in the minds of residents the idea that significant tsunami danger would require shaking even stronger than during the 2009 earthquake.

Only 13 months later, however, the 2010 earthquake took place seaward of the Mentawai Islands, generating a catastrophic tsunami with a run-up of 17 meters that caused seven hundred deaths on the islands (Hill et al. 2012). This event, which can be construed as an aftershock of the 2007 Bengkulu earthquake to the south, was clearly a "tsunami earthquake," felt at deceptively low levels on the islands, and was later identified as such in a number of seismological studies (Newman et al. 2011; Saloor and Okal 2018). Thus, and tragically, these two events of 2009 and 2010 were both anomalous, but in opposite ways; the 2009 fast event caused enhanced dynamic destruction and death, and the 2010 slow one caused an enhanced tsunami.

Based on reports from survivors who described the 2010 Mentawai event as a "gentle, slow, rocking earthquake that lasted for several minutes" (Hill et al. 2012, 4) and on the work of Convers and Newman (2011), who pointed out its anomalous character within 17 minutes of origin time based on a comparison of the duration and energy of teleseismic *P* waves, this tsunami earthquake would suggest amending the near-field recommendation to "the shaking, *strong or long*, is the warning." The task of issuing a warning, however, runs into the immense difficulty of defining an appropriate level of duration using a qualitative perception of time by lay populations.

In this very general context, a prototype experiment took place in the spring of 2016, when a sensor was deployed for slightly less than two months in the Mentawai Basin. This experiment is the subject of this chapter.

Operational Aspects

Our 2016 experiment consisted of operating a pressure sensor on the bottom of the Mentawai Channel. The technology of the instrument in use is conceptually similar to that of the so-called deep-ocean assessment and reporting of tsunamis (DART) buoys (Meining et al. 2005). Ours, however, is designed to be used in the near field, in the immediate epicentral area. In addition, instead of transmitting via acoustic modem to a nearby surface buoy, our system transmits over distances of 20 to 30 kilometers to a seafloor station cabled to shore. The motivation for such a long-range acoustic link is to eliminate the need for a surface buoy, which requires maintenance and is subject to damage from ocean forces or vandalism (Teng et al. 2010; Mungov et al. 2013).

In addition, we recall that DART buoys operate at a sampling rate of $\delta t = 15$ seconds, that particular channel being triggered for real-time transmission only upon detection of a large event. By contrast, our system uses a much shorter time sampling of $\delta t \approx 0.05$ second, with the real-time transmission of the full dataset made possible by the elimination of the buoy relay. That short time sampling allows a full broadband seismic processing of the time series, in contrast to the coarse sampling used by DART buoys. A permanent seafloor sensor will still require regular maintenance including battery changes, so minimizing energy use is critical. This limitation then mandated the use of a single pressure sensor as opposed to a complete broadband motion package such as those

employed in standard ocean bottom seismometers. In this regard, it is desirable to extract as much useful information as possible from the pressure sensor, including the magnitude of seismic waves impinging on the ocean bottom unit. The work presented here reviews the results of an initial approach toward that use.

The instrumental package was deployed in the Mentawai Basin on March 23, 2016, in the vicinity of 1.350°S, 99.733°E at a of depth $H \approx$ 1,750 meters (hereafter Mentawai Basin site or MBS).[2] The above coordinates refer to the sea surface location where the instrument was dropped, which is estimated to coincide with its resting position within uncertainties on the order of a few hundred meters. The exact depth of deployment was provided by the sensor itself. The instrument was retrieved on May 16, 2016, and provided a continuous stream of data from March 26 to May 12, 2016, that is, for forty-eight days.

The instrument deployed consists of a Paroscientific Digiquartz nanoresolution pressure sensor model 8CB2000-I, which includes preprocessing of the native frequency output so that the data are available as an ASCII serial data stream (Paros et al. 2012). The package was deployed on a platform resting on the seafloor and consisted of a pressure sensor, a data logger, a battery, and an acoustic release for recovery.[3] The platform, called a lander because it rests directly on the seafloor, is deployed from a surface vessel and free-falls to the bottom.

Recording was performed at a sampling rate of twenty-two samples per second. The raw data were stored as a pressure time series expressed in pounds[-force] per square inch (psi), later converted to metric units through the factor

$$1 \text{ psi} = 68972 \text{ dyn} \times \text{cm}^2 = 6897.2 \text{ Pa} \qquad (1)$$

Figure 9-1 is an example of a 24-hour time series obtained for April 13, 2016, containing the record of an earthquake in Myanmar (hereafter event T4), with an intermediate depth of 136 kilometers and moment magnitude $M_w = 6.9$ (Kanamori 1977). It is easily verified that the average value recorded ($\sim$ 2,550 psi) is the hydrostatic pressure of the water column at the site, $p = \rho_w g H$, which translates to a depth $H = 1{,}744$ meters using a density $\rho_w = 1.03$ g/cm^3 and the acceleration of gravity $g = 979$ cm/s^2, which is appropriate near the equator. In addition, the large oscillation shown in figure 9-1 is the tidal signal, whose peak-to-peak amplitude, typically 1.15 psi, translates into an amplitude of 79 centimeters for the oceanic tide. This amplitude compares favorably with

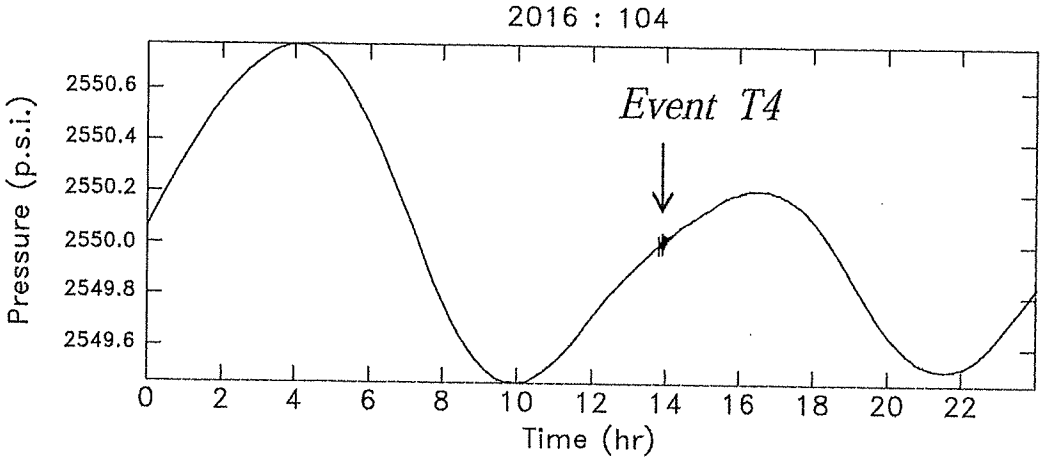

FIGURE 9-1. Example of raw 24-hour time series recorded at the Mentawai Basin site on April 13, 2016. The main oscillation expresses the tide. The signal around 14:00 GMT is Event T4, an intermediate-depth earthquake in Myanmar.

tides typically on the order of 1.2 meters peak to peak in the port of Padang, given the expected influence of the response of the harbor. These observations provide an independent check of the proper calibration of the instrument.

Data Processing

Data processing includes both plotting the raw data from the seismometer and analyzing the spectra to detect seismic events. This process integrates visualization and interpretation of the data to assess the type and size of seismic waves generated by an earthquake with potential tsunami risk and translates the seismic signals into a form that is understood by scientists and practicing emergency managers.

Raw spectra

Figure 9-2 presents the spectrum of a one-day-long window of data, recorded in the absence of detectable seismic signals, on April 9, 2016. In lay terms, it plots the energy recorded by the sensor as background noise, as a function of frequency, from "bass" at the left of the diagram to "treble" at the right. For reference, we compare it to the spectrum of the vertical broadband seismometer at the station GSI, operated by GEOFON at Gunungsitoli, on nearby Nias Island, the distance between the two sites being 380 kilometers.

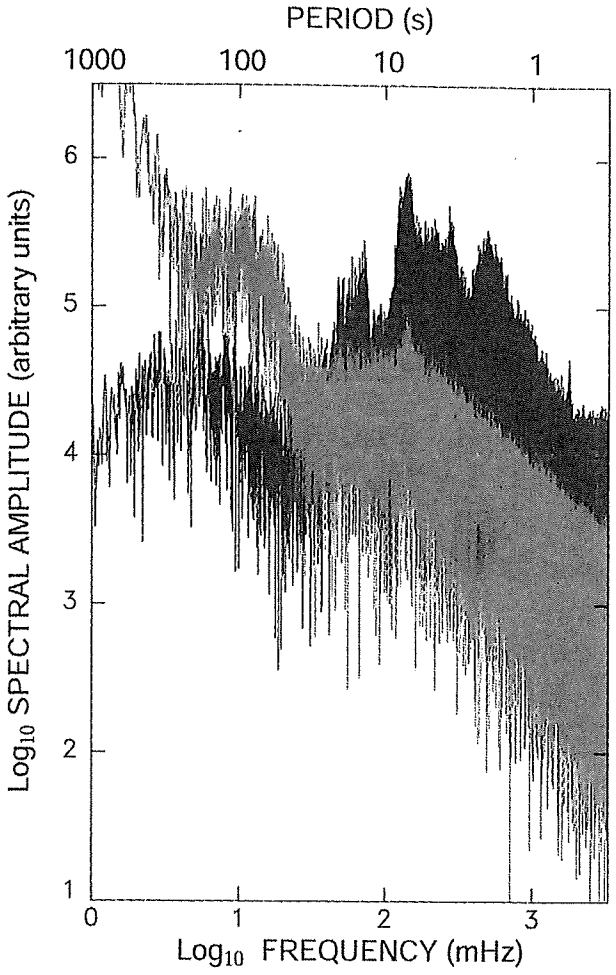

FIGURE 9-2. Spectral amplitude (in grey) of 24-hour record at MBS in the absence of seismic signal (09 April 2016). For reference, the corresponding spectrum at the nearby GEOFON station GSI is given in black. The vertical scales for logarithmic units are common to both plots, but their baselines are different, allowing for direct comparison of the repartition of background noise across the frequency spectrum. Note strong noise at MBS for $T \geq 30$s.

These spectra have not been corrected for instrument response because, in the case of the pressure sensor and as discussed below, the conversion to ground motion involves different functions depending on the nature of the particular seismic wave recorded. Rather, figure 9-2 simply explores the level of background noise, and hence the feasibility of extracting seismic signals in various frequency bands. The vertical scales are common logarithmic units, but unrelated in an absolute sense, thus allowing a *relative* comparison of the levels of background noise as a function of frequency.

Between 0.1 and 10 Hz, corresponding to periods of 10 to 0.1 seconds, the land site GSI is dominated by microseismic noise due to the harmonics of sea swell, peaked around 6 seconds, a ubiquitous feature of coastal seismic stations (Brune and Oliver 1959; Berger et al. 2004; McNamara and Buland 2004). By contrast, and expectedly, these harmonics are absent from the seafloor record, as is the fundamental of the swell, around 12 seconds, thus illustrating the well-known property that submarines do

not "feel" the weather, whose relatively short waves fail to penetrate deep into the water column.

Although the noise at the seafloor site is relatively low beyond 30 millihertz, it increases substantially at lower frequencies, in sharp contrast to the seismic spectrum at GSI. This increase will, unfortunately, prevent a quantitative interpretation of surface waves at periods $T \geq 30$ seconds. The origin of this effect is presently unknown.

Spectrogram analysis and detection of seismic events

All forty-eight available 24-hour time windows of data were submitted to a classical spectrogram analysis (Cohen 1989). In simple terms, this procedure isolates a narrow window (in this case, 100 seconds long) moving across the time series (in this case, in steps of 50 seconds) and applies a classic spectral analysis (in our case, between 2 and 10 hertz). The resulting spectral amplitude, computed as in figure 9-2, is then color-coded in decibels with respect to its maximum, with each pixel characterizing the amount of energy present at a given time (abscissa) and frequency (ordinate).[4]

This procedure has been used in various seismological applications for several decades (e.g., Okal and Talandier 1997). Its power is that it allows the systematic detection of small events, which would fail a simple visual investigation, as exemplified by a dynamic profile for the one-day window spanning April 10, 2016: while a small local event, which took place in South Sumatra (hereafter event L2), is clearly visible about 9,000 seconds into the time series, the spectrogram reveals a second earthquake at ~38,000 seconds that would otherwise not emerge from the background noise.

Processing of Teleseismic Events

We call "teleseismic" those earthquakes that occur at a distance of more than 1,000 kilometers from the receiver. Eight such events, listed in table 9-1 and mapped in figure 9-3, were detected on spectrograms in our experiment. Their seismic moments range from 1.1×10^{25} dyn × cm ($M_w = 6.0$) for event T5, a small earthquake in Mindanao, to 5.9×10^{27} dyn × cm (M_w=7.8) for event T7, the large 2016 Muisne, Ecuador, earthquake. It is noteworthy that the epicenter of event T7 was essentially antipodal to MBS (the angular distance Δ as seen from the center of the Earth between source and receiver being 178.95° out of a maximum 180°).

TABLE 9-1. Teleseismic events recorded in this study

Code	Date D	M	(J)	Y	Origin Time GMT	Epicenter (°N)	(°E)	Depth (km)	Global Values M_0[a]	M_s	Θ	Distance (°)	Local Estimates M_s	E^{Ea}	Θ	Region
T1	03	APR	(094)	2016	08:23:52	−14.32	166.85	26	22	6.8	−4.89	67.51	6.7	35.9	−4.79	Vanuatu
T2	06	APR	(097)	2016	14:45:30	−8.20	107.39	29	1.5	5.4	−4.92	10.2	5.4	2.67	−4.75	Java
T3	10	APR	(101)	2016	10:28:59	36.47	71.13	212	11		−4.34	46.15		23.5	−4.67	Hindu Kush (Intermediate)
T4	13	APR	(104)	2016	13:55:18	23.10	94.68	136	32		−4.46	24.87		114	−4.45	Myanmar (Intermediate)
T5	13	APR	(104)	2016	18:21:53	7.79	122.02	17	1.1	5.6	−4.96	24.02	5.7	0.82	−5.13	Mindanao, Philippines
T6	15	APR	(106)	2016	16:25:06	32.79	130.75	10	45	7.3	−5.00	44.90	7.2	27.2	−5.22	Kyushu
T7	16	APR	(107)	2016	23:58:37	0.35	−79.93	21	590	7.5	−5.15	178.95				Ecuador
T8	28	APR	(119)	2016	19:33:24	−16.04	167.38	24	36	7.1	−4.71	68.16	6.9	167	−4.33	Vanuatu

[a]Moment values are in units of 10^{25} dyn × cm, and estimated energies are in 10^{20} erg.

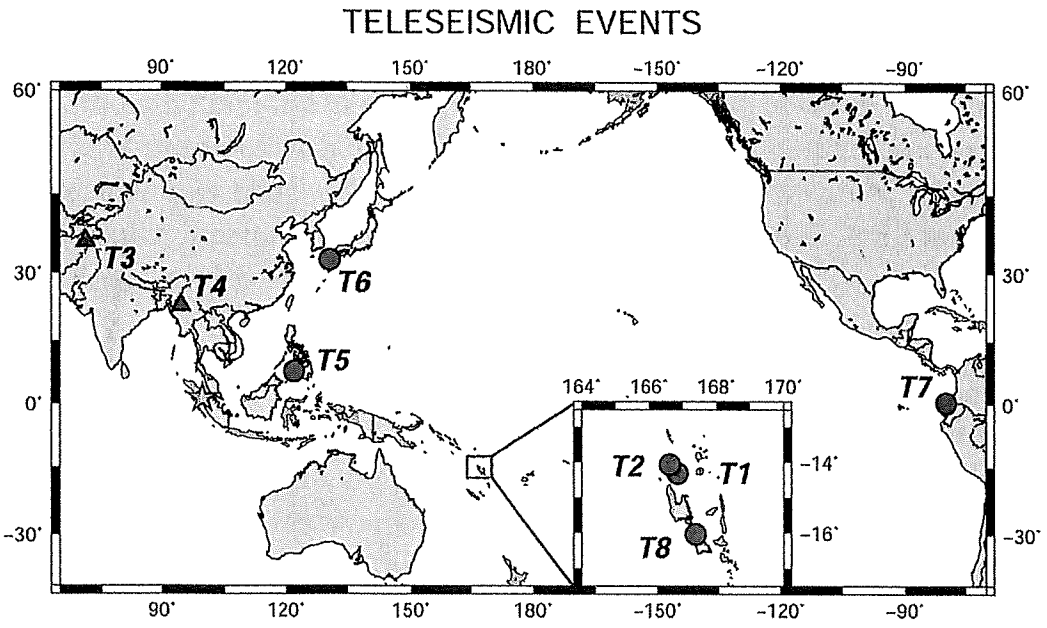

FIGURE 9-3. Map of epicenters of earthquakes detected at teleseismic distances by the hydrophone at the Mentawai Basin site (star). Shallow events ($h < 70$ km) are shown as full circles, and intermediate ones are shown as triangles. See table 9-1 for information on codes T1–T8.

Rayleigh waves

To examine the long-period properties of our records, we first focus on Rayleigh waves, a class of surface waves creeping along the circumference of Earth and prominent at periods of 10 to several hundred seconds (Stein and Wysession 1991). Elementary seismic theory (e.g., Haskell 1953) shows that a pressure sensor at the interface between a solid half-space and an ocean of thickness H records a Rayleigh wave as an overpressure of amplitude

$$P = \rho_w \omega^2 H \cdot u_z \qquad (2)$$

where u_z is the vertical seismic displacement of the solid Earth and $\omega = 2\pi/T$ is the angular frequency of the wave of period T. In other words, the pressure sensor functions as an accelerometer whose gain is proportional to the depth of the water column. At a depth of 1,750 meters, the vertical displacement of the Rayleigh wave can be restored by first converting the digital values (pounds-force per square inch) to metric units (dyn/cm^2) and then representing the sensor as an instrument featuring two null "zeros" and no poles (Aki and Richards 2002, 637),

with a total magnification of $-\rho_w H = -1{,}802{,}000$ kilograms per square meter. In simple terms, this procedure allows us to transform the signal detected by the sensor (in units of pressure) into a quantitative measurement of the amplitude of the Rayleigh wave (in units of length).

Because of the excessive noise at periods longer than 30 seconds (figure 9-2), it was not possible to compute mantle magnitudes (Okal and Talandier 1989), which would have allowed the retrieval of a long-period seismic moment at periods of several hundred seconds. Rather, we had to limit our investigations to conventional surface-wave magnitudes, using the Prague formula for Rayleigh waves with a period T close to 20 seconds (Vaněk et al. 1962):

$$M_s = \log_{10}\left(\frac{A}{T}\right) + 1.66 \log_{10}\Delta + 3.3 \qquad (3)$$

where A is in microns, T in seconds, and Δ in degrees. For each record, we extract a 1-hour time window containing the Rayleigh wave train and filter it between 10 and 30 seconds. A time-domain measurement of the maximum amplitude can be converted into a displacement using equation (2), which substituted into equation (3) leads to

$$M_s = \log_{10}(p \cdot T) + 1.66 \log_{10}\Delta + 5.3 \qquad (4)$$

where p is in psi. Figure 9-4 shows that the records of teleseismic events are comparable to standard seismograms and illustrates the measurement of M_s according to equation (4). As detailed in table 9-1, we obtain M_s values in excellent agreement with published ones; note that we do not compute M_s for events T3 and T4, which are at intermediate depths where 20-second surface waves are poorly excited, nor for T7, for which the station is antipodal ($\Delta \approx 179°$).

We conclude that the pressure sensor can be used reliably to quantify the amplitude of conventional 20-second Rayleigh waves from teleseismic events in the range $M_s = 5.4$ to 7.2. Unfortunately, the only significantly larger event recorded during our deployment was antipodal; also, the presence of unexplained but substantial noise at longer periods prevented the extension of our investigations to the domain of mantle waves more directly associated with tsunami excitation.

P waves

P (for "primary") waves are seismic body waves, traveling from a source to a receiver through the Earth's interior ("body") (Stein and Wysession

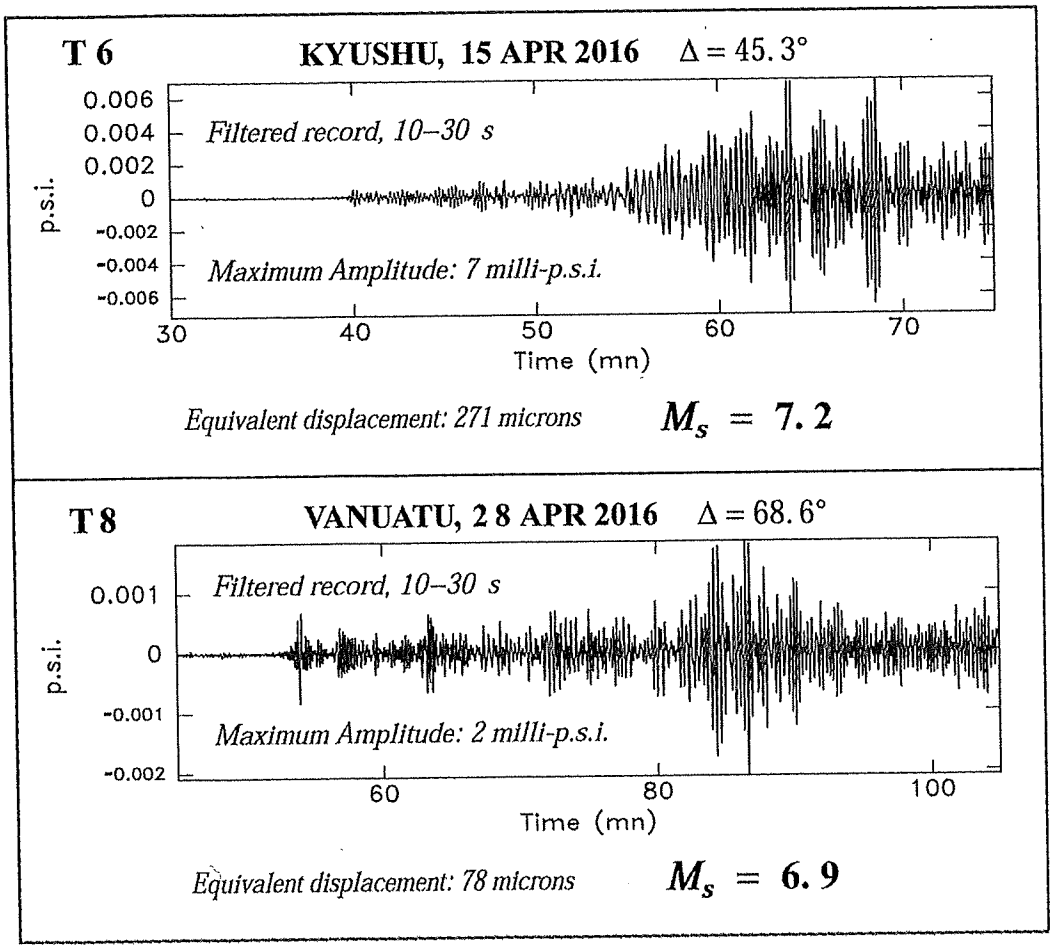

FIGURE 9-4. Examples of computation of surface-wave magnitude M_s at the Mentawai Basin site for teleseismic events T6 (Kyushu) and T8 (Vanuatu). See text for details.

1991). They constitute the fastest signals reaching a distant station, in practice a few minutes after origin time. They are also least attenuated during their propagation and as such carry significant energy even at short periods, typically on the order of 1 second.

Here, we use *P* waves recorded by our ocean bottom pressure sensor from teleseismic events to compute an energy flux at the receiver, and from there an estimate of the seismic energy radiated by the source, following the algorithm of Newman and Okal (1998), itself inspired by Boatwright and Choy (1986). Such measurements constitute a quantification of the earthquake at the high-frequency end of its source spectrum.

At the bottom of a liquid layer where the sound velocity is α_w, it can be shown that, upon incidence of a *P* wave, the ratio of pressure in the fluid to vertical displacement at the interface (known in physics as an impedance) is

$$Z = \frac{p}{u_z} = \rho_w \alpha_w \omega \tag{5}$$

This formula shows that a pressure sensor responds differently to Rayleigh waves and *P* waves. Whereas in the former case it behaved as an accelerometer, it will now respond to ground velocity, which amounts to adding a factor $(\alpha_w/\omega H)$ to the response used above for surface waves.

The computation of radiated energy proceeds along the steps detailed by Newman and Okal (1998) and routinely implemented since then, but an additional complexity stems from multiple reverberations in the water column (figure 9-5). As an incident seismic wave impinges on the surface of the Earth, it undergoes significant transformations to prevent its continuation into the atmosphere (conveniently taken as a vacuum), which can be regarded as a relatively complex extension of the principle of an optical mirror. As a consequence, the field of ground motion is altered at the free surface, requiring a correction in the computation of the teleseismic energy flux, noted $C^p(i_0)$ in Newman and Okal (1998), and whose detailed expression is given, for example, by Okal (1992). In the oceanic environment, the water layer traps a fraction of the energy in a frequency-dependent process reminiscent of the effect of coating in the conception of partial mirrors. It can be considered the conjugate, at the receiver, of the well-known source-side generation of multiply reflected *pmwP* phases (Mendiguren 1971). At the high frequencies characteristic of *P* waves, it is appropriate to sum the energies of the various rays involved in

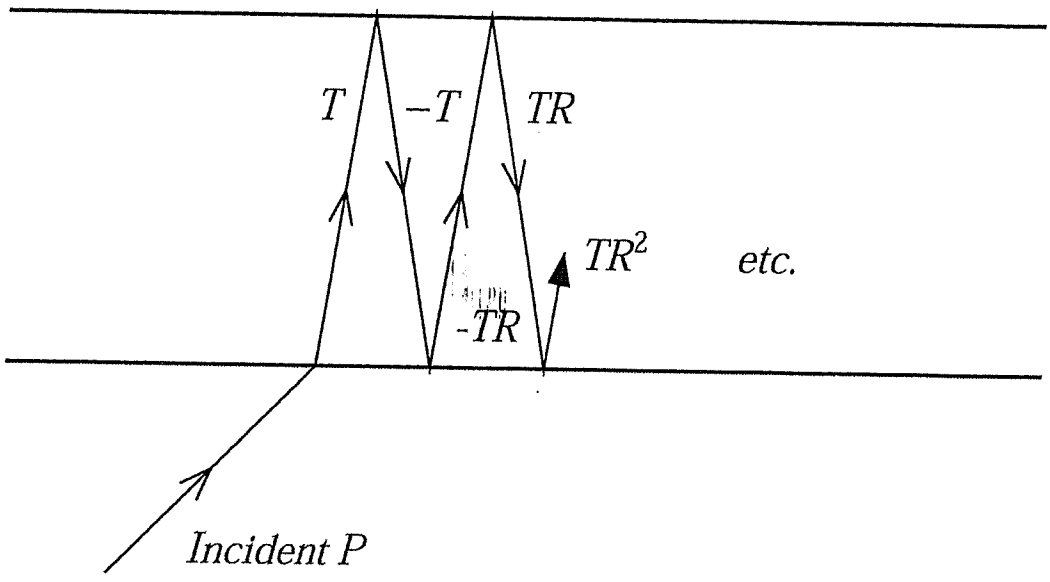

FIGURE 9-5. Multiple reflections and response function of the oceanic column for a teleseismic *P* wave recorded as a pressure signal at the bottom of the ocean. See text for details.

the multiple reflections (see figure 9-5), and the classical surface response coefficient for incident *P* waves, used by Newman and Okal (1998), must be replaced by a more complex one, whose detailed expression is derived in Okal and Freitag (2020). Finally, a special algorithm is used for events T3 and T4, whose depths are intermediate (Saloor and Okal 2018), and an additional correction effected for events T2, T4, and T5, for which the station is less than 30° away (Ebeling and Okal 2012).

Table 9-1 includes values of the resulting estimated energies E^E for seven teleseismic events (the computation is not carried out for the antipodal event T7), as well as parameters $\Theta = \log_{10}(E^E/M_0)$, obtained using published values of the seismic moments M_0 of the relevant earthquakes. These values are compared to values of Θ computed routinely from a global dataset of stations (Newman and Okal 1998; Saloor and Okal 2018). As shown in figure 9-6, the agreement is excellent, with no systematic trend in the residual between the value of Θ obtained here from the pressure sensor and its reference value; as for the root-mean-square of the residual (0.22 logarithmic unit), it is comparable to the scatter of individual station values when using large global datasets at seismological stations. Our results thus validate the use of the pressure sensor to

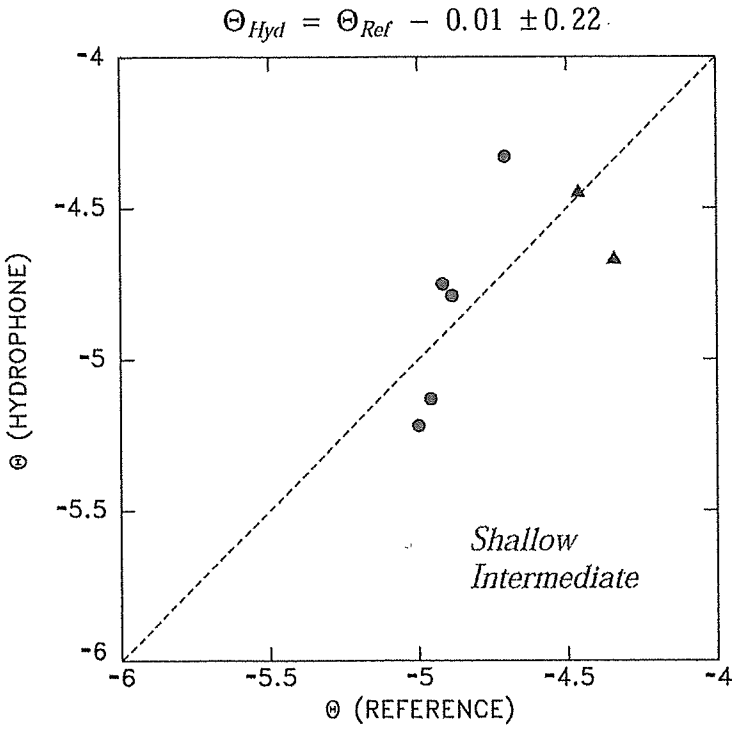

FIGURE 9-6. Comparison of values of the slowness parameters Θ obtained from a global dataset (abscissa) and from the hydrophone at the Mentawai Basin site (ordinate).

quantify a teleseismic source at the higher-frequency end of the seismic spectrum.

Processing of Local Events

Six regional earthquakes, listed in table 9-2 and mapped in figure 9-7, were detected from spectrograms in the present experiment. Two of them, events L1 and L5, took place at intermediate depths of 160 and 115 kilometers, respectively, in the down-going slab under Sumatra. Except for the small event L6, also closest to the sensor at only 58 kilometers, all had a moment tensor inverted as part of the Global Centroid-Moment-Tensor, or Global CMT, Project (Dziewonski et al. 1981; Ekström et al. 2012), with moments listed in table 9-2.

Also shown in figure 9-7 are "beachball" diagrams of the relevant moment tensors, which offer a conventional representation of the geometry of faulting of the earthquake source (Stein and Wysession 1991). Note the diversity in focal geometries, which illustrates the oblique convergence at the Sumatra trench (Sella et al. 2002).

At such regional distances, the formalism of Newman and Okal (1998) no longer applies, and an estimate of earthquake energy must be obtained through an alternate computation. A simple approach consists of directly integrating the energy flux of the time series of overpressure. By analogy with energy estimates computed at teleseismic distances (Boatwright and Choy 1986; Newman and Okal 1998), we simply consider the pressure flux

$$F_P = \frac{\alpha_w}{\pi} \int \frac{|P|^2(\omega)}{K} \cdot d\omega \qquad (6)$$

where $P(\omega)$ is the Fourier transform of the pressure $p(t)$ and where α_ω and K are the sound velocity and bulk modulus of the water, respectively; again by analogy with computations of estimated energy, the integral in equation (6) is conveniently limited to the window 0.1 to 2 hertz. Note that we neglect anelastic attenuation at regional distances. Through a further, and admittedly drastic simplification, an estimate of the total energy of the seismic source is then obtained by scaling F_P to the square of the epicentral distance D and weighting the result to include the contribution of S waves to obtain a pressure-estimated energy

$$E_P^E = 4\pi \cdot D^2 \cdot (1 + q^{BC}) \cdot F_P \qquad (7)$$

TABLE 9-2. Local events recorded in this study

Code	Date D	M	(J)	Y	Origin Time GMT	Epicenter (°N)	(°E)	Depth (km)	Global Values M_0^a	m_b	Distance (km)	Local Estimates F_P^a	E_P^{Ea}	Θ_P	Region
L1	29	MAR	(089)	2016	06:24:48	–2.807	102.319	160	8.4	5.1	329.9	24.6	0.56	–5.18	Southern Sumatra (Intermediate)
L2	10	APR	(101)	2016	02:14:35	–4.149	102.211	41	46	6.0	414.9	194.	6.99	–4.57	Southern Sumatra
L3	15	APR	(106)	2016	10:24:31	–3.620	100.492	38	5.8	4.7	265.3	12.4	0.21	–5.47	Southern Sumatra
L4	16	APR	(107)	2016	21:09:12	0.450	97.971	10	2.1	5.1	279.7	6.84	0.11	–5.25	Northern Sumatra
L5	02	MAY	(123)	2016	04:21:25	–4.989	104.551	115	47	6.0	669.8	32.7	3.06	–5.19	Southern Sumatra (Intermediate)
L6	03	MAY	(124)	2016	22:32:36	–1.875	99.734	35	*2.9*[b]	4.5	58.2	3.30	0.20	*–5.16*[b]	Southern Sumatra

[a]Moment values are in in units of 10^{23} dyn × cm, fluxes are in g/s^2, and estimated energies are in 10^{19} erg.

[b]For Event L6, values in italics are estimated from scaling laws (Geller 1976; Okal 2019).

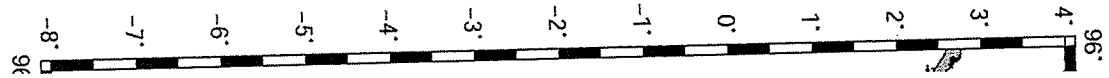

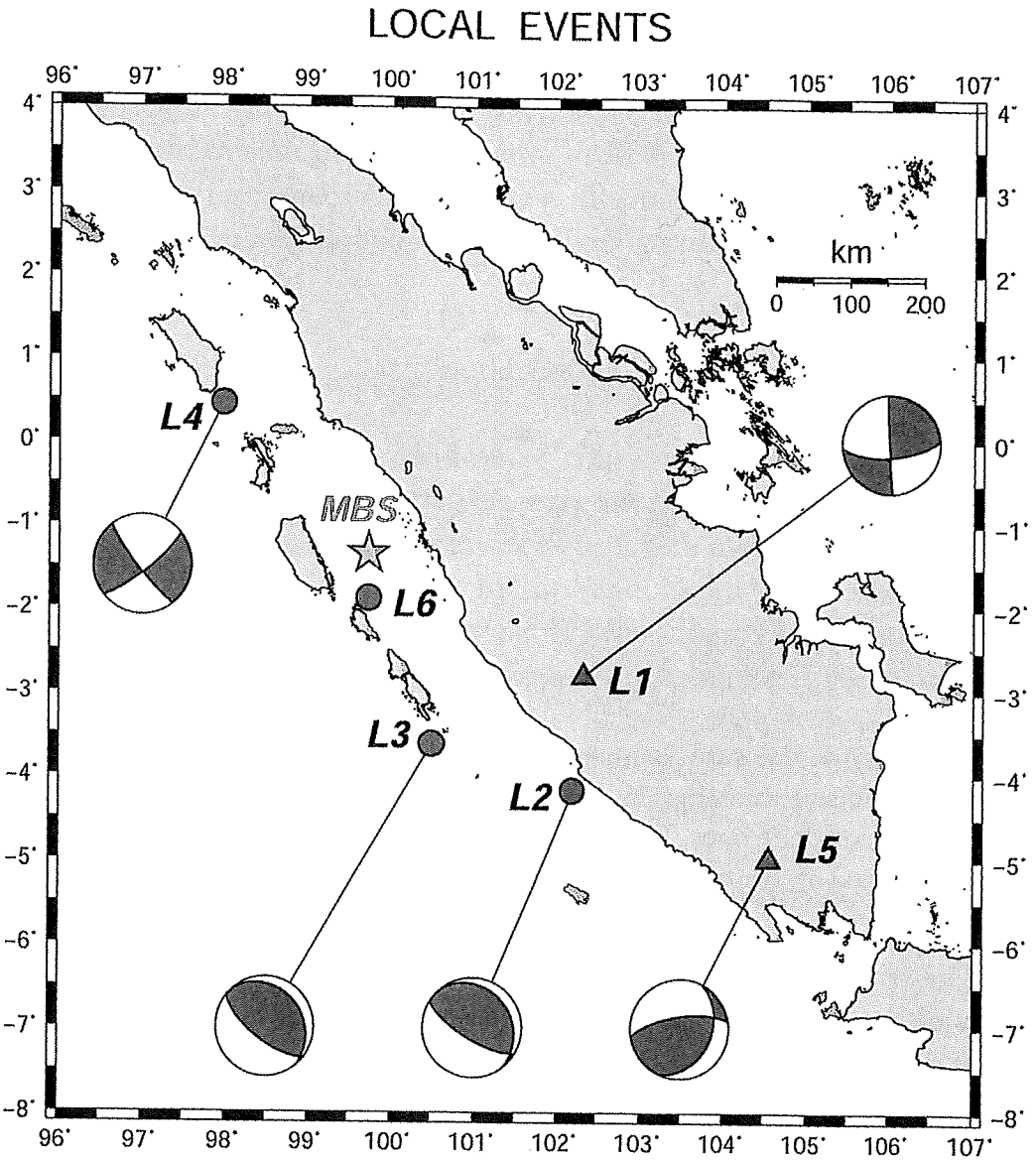

FIGURE 9-7. Map of the epicenters of local earthquakes detected at regional distances by the hydrophone at the Mentawai Basin site (star). Shallow events ($h <$ 70 km) are shown as full circles, and intermediate ones are shown as triangles. See table 9-2 for information on codes L1–L6. Also shown are global CMT solutions, except for event L6.

where q^{BC} is given by Newman and Okal (1998) after Boatwright and Choy (1986). For event L6, at a distance smaller than 100 kilometers, the far-field approximation to the body wavefield inherent in those authors' formalism breaks down (Aki and Richards 2002, section 4.3), and D is replaced in the near field by $D^{NF} = 2\pi D^2/\Lambda$, where the wavelength $\Lambda =$ 40 kilometers is computed at a typical period of 5 seconds.

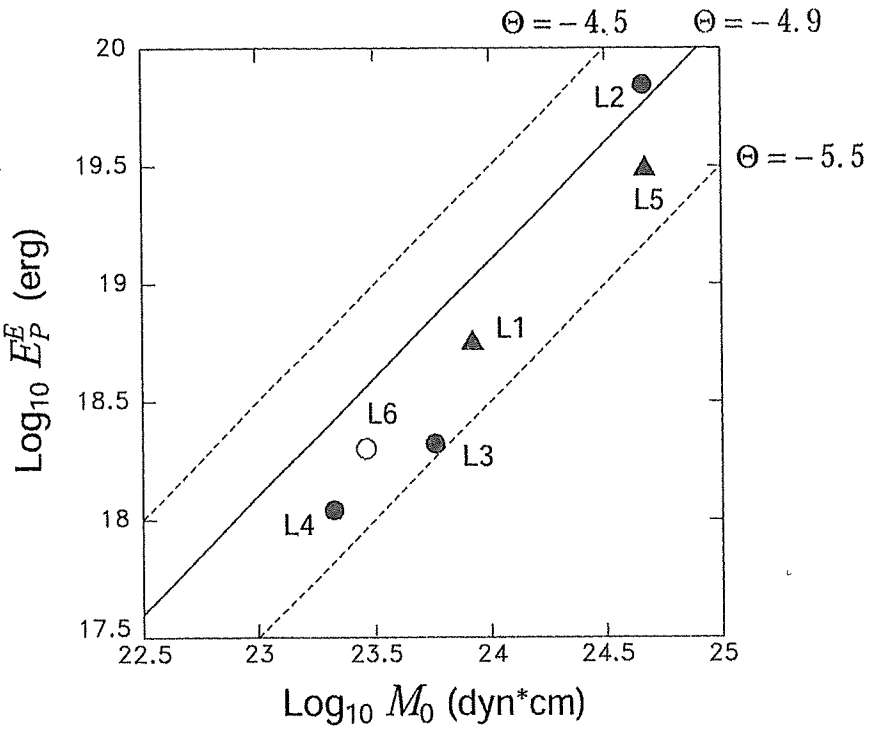

FIGURE 9-8. Pressure-estimated seismic energy E_p^E at MBS *vs.* published seismic moment M_0. Circles refer to shallow events, triangles to intermediate ones. The open circle is event L6, whose moment is estimated on the basis of its body-wave magnitude m_b.

The results are listed in table 9-2, where E_p^E is scaled to the published M_0, yielding a pressure-estimated energy-to-moment parameter Θ_p. Figure 9-8 plots E_P^E versus published moment M_0.

It is not possible to compare directly Θ_p to values of Θ computed from seismograms at teleseismic distances because the regional events detected during our deployment are too small ($M_0 \leq 4.7 \times 10^{23}$ dyn * cm; $M_w \leq 5.7$) to lend themselves to a routine global computation of Θ. Nevertheless, it is remarkable that this range of computed values of Θ_p (−4.57 to −5.47) is typical of values measured at subduction zones (Okal and Newman 1998). In the case of the smallest (and closest) event L6, for which no seismic moment is available, a tentative value of $M_0 = 2.9 \times 10^{23}$ dyn * cm ($M_w = 4.9$) can be estimated by scaling the moment of event L3 using the difference of body wave magnitudes (4.5 versus 4.7), in a range of sizes where m_b has started to saturate (Geller 1976; Okal 2019), and under the assumption that those events follow scaling laws. The result is a tentative value of $\Theta_p = -5.18$, again in excellent agreement with values expected at subduction zones, confirming that an estimate of high-frequency quantification of seismic sources in the near field can be obtained, even at very short distances and for small events.

In summary, this experiment with pressure records of regional earthquakes shows that it is feasible to obtain quantitative estimates of the size of seismic sources. In practice, we did not catch any obviously anomalous regional earthquakes during our short-lived experiment. We emphasize, however, that the events detected were all small by global seismological standards, and, *a fortiori*, had no tsunamigenic potential.

Conclusion

During a forty-eight-day window of continuous operations, we were able to detect fourteen earthquakes—six at regional distances and eight global events at teleseismic distances—for which meaningful quantifications of the seismic source were obtained and, for all but one small event, successfully compared to globally published values. These results verify the concept of using a seafloor pressure sensor to quantify the source of a seismic event, particularly in the near field, even though the presence of unexpected noise at periods longer than 30 seconds restricts the recovery of the longest-period part of the seismic spectrum.

There remains the caveat that, given the short nature of our experiment, neither a truly large earthquake (except the antipodal Ecuadorian event T7), nor a significant local one, was detected at MBS. In particular, none of the fourteen events generated any gravitational water wave detectable by our pressure sensor. Only the continuous operation of the sensor over a much longer period of time will allow us to eventually expand our investigation to this condition, in fulfillment of the motivation of our project.

Acknowledgments

This research was supported by the Hazards SEES program of the National Science Foundation under Grant Number OCE-1331463 to the University of Pittsburgh. We thank Louise Comfort for her leadership in this project. The authors would like to acknowledge the invaluable help of Professor Febrin Anas Ismail of Andalas University (Padang), Iyan Turyana of the BPPT (Jakarta), and the captain and crew of the *KN MUCI* (Padang). The Woods Hole Oceanographic Institution field team included engineers Peter Koski and Keenan Ball with additional support from Sandipa Singh and James Partan. Some figures were plotted using the GMT software (Wessel and Smith 1991).

Notes

1. Incidentally, a very similar situation exists regarding hurricanes, commonly classified into "categories" (ranging from 1 to 5) supposedly describing all their properties (size of the system, maximum wind velocity, underpressure at the center of the eye). Recent cases (e.g., Hurricanes Sandy in 2012 and Patricia in 2015) have shown that these properties are not always correlated and that a classification using a single category number constitutes a significant, and potentially hazardous, oversimplification.

2. A map showing the location of the Mentawai Basin site can be found in the Resources tab at islandpress.org/hazardous-seas.

3. A photo of this undersea unit is available in the Resources tab at islandpress.org/hazardous-seas.

4. A color-coded dynamic profile for the one-day window of April 10, 2016, can be found in the Resources tab at islandpress.org/hazardous-seas.

References

Abe, Kuniaki, Katsuyuki Abe, Yoshinobu Tsuji, Fumihiko Imamura, H. Katao, I. Yohihisa, Kenji Satake, Joanne Bourgeois, E. Noguera, and F. Estrada. 1993. "Field survey of the Nicaragua earthquake and tsunami of September 2, 1992." *Bulletin of the Earthquake Research Institute, University of Tokyo* 68, no. 1: 23–70.

Aki, Keiiti. 1966. "Generation and Propagation of G Waves from the Niigata Earthquake of June 16, 1964.: Part 2. Estimation of earthquake moment, released energy, and stress-strain drop from the G wave spectrum." *Bulletin of the Earthquake Research Institute, University of Tokyo* 44, no. 1: 73–88.

Aki, Keiiti, and Paul G. Richards. 2002. *Quantitative Seismology*, 2nd ed. Sausalito, CA: Univ. Science Books, 218–35.

Berger, Jonathan, Peter Davis, and Göran Ekström. 2004. "Ambient Earth noise: A survey of the global seismographic network." *Journal of Geophysical Research: Solid Earth* 109, no. B11: B11307, 10 pp.

Boatwright, John, and George L. Choy. 1986. "Teleseismic estimates of the energy radiated by shallow earthquakes." *Journal of Geophysical Research: Solid Earth* 91, no. B2: 2095–112.

Borrero, José C., Kerry Sieh, Mohamed Chlieh, and Costas E. Synolakis. 2006. "Tsunami inundation modeling for western Sumatra." *Proceedings of the National Academy of Sciences* 103, no. 52: 19673–77.

Borrero, José C., Robert Weiss, Emile A. Okal, Rahman Hidayat, Suranto, Diego Arcas, and Vasily V. Titov. 2009. "The tsunami of 2007 September 12, Bengkulu province, Sumatra, Indonesia: Post-tsunami field survey and numerical modelling." *Geophysical Journal International* 178, no. 1: 180–94.

Bothara, Jitendra, Dick Beetham, Dave Brunsdon, Mike Stannard, Roger Brown, Clark Hyland, Warren Lewis, Scott Miller, Rebecca Sanders, and Yakso Sulistio. 2010. "General observations of effects of the 30th September 2009 Padang earthquake, Indonesia." *Bulletin of the New Zealand Society for Earthquake Engineering* 43, no. 3: 143–73.

Brune, James N., and Jack Oliver. 1959. "The seismic noise of the Earth's surface." *Bulletin of the Seismological Society of America* 49, no. 4: 349–53.

Choy, George L., and John L. Boatwright. 1995. "Global patterns of radiated seismic energy and apparent stress." *Journal of Geophysical Research: Solid Earth* 100, no. B9: 18205–28.

Cohen, Leon. 1989. "Time-frequency distributions—a review." *Proceedings of the Institute of Electrical Electronic Engineering* 77, no. 7: 941–81.

Convers, Jaime Andres, and Andrew V. Newman. 2013. "Rapid earthquake rupture duration esti-

mates from teleseismic energy rates, with application to real-time warning." *Geophysical Research Letters* 40, no. 22: 5844–48.

Dziewonski, Adam M., T.-A. Chou, and John H. Woodhouse. 1981. "Determination of earthquake source parameters from waveform data for studies of global and regional seismicity." *Journal of Geophysical Research: Solid Earth* 86, no. B4: 2825–52.

Ebeling, Carl W., and Emile A. Okal. 2012. "An extension of the E/M_0 tsunami earthquake discriminant Θ to regional distances." *Geophysical Journal International* 190, no. 3: 1640–56.

Ekström, Göran, Meredith Nettles, and Adam M. Dziewoński. 2012. "The Global CMT Project 2004–2010: Centroid-moment tensors for 13,017 earthquakes." *Physics of the Earth and Planetary Interiors* 200: 1–9.

Freitag, L., and E. A. Okal. 2020. "Preliminary results from a prototype ocean-bottom pressure sensor deployed in the Mentawai Channel, Central Sumatra, Indonesia." *Pure and Applied Geophysics* 177: 5119–31. https://doi.org/10.1007/s00024-020-02561-6.

Fukao, Yoshio. 1979. "Tsunami earthquakes and subduction processes near deep-sea trenches." *Journal of Geophysical Research: Solid Earth* 84, no. B5: 2303–14.

Geller, Robert J. 1976. "Scaling relations for earthquake source parameters and magnitudes." *Bulletin of the Seismological Society of America* 66, no. 5: 1501–23.

Gutenberg, Beno. 1945. "Magnitude determination for deep-focus earthquakes." *Bulletin of the Seismological Society of America* 35, no. 3: 117–30.

Haskell, N. A. 1953. "The dispersion of surface waves on multilayered media." *Bulletin of the Seismological Society of America* 43: 17–34.

Hill, Emma M., José C. Borrero, Zhenhua Huang, Qiang Qiu, Paramesh Banerjee, Danny H. Natawidjaja, Pedro Elosegui, et al. 2012. "The 2010 M_w = 7.8 Mentawai earthquake: Very shallow source of a rare tsunami earthquake determined from tsunami field survey and near-field GPS data." *Journal of Geophysical Research: Solid Earth* 117, no. B6: B06402, 21 pp.

Ide, Satoshi, and Gregory C. Beroza. 2001. "Does apparent stress vary with earthquake size?" *Geophysical Research Letters* 28, no. 17: 3349–52.

Kaiser, A., C. Holden, J. Beavan, D. Beetham, R. Benites, A. Celentano, D. Collett, et al. 2012. "The M_w = 6.2 Christchurch earthquake of February 2011: Preliminary report." *New Zealand Journal of Geology and Geophysics* 55, no. 1: 67–90.

Kanamori, Hiroo. 1972. "Mechanism of tsunami earthquakes." *Physics of the Earth and Planetary Interiors* 6, no. 5: 346–59.

Kanamori, Hiroo. 1977. "The energy release in great earthquakes." *Journal of Geophysical Research* 82, no. 20: 2981–87.

Kanamori, Hiroo, and Luis Rivera. 2008. "Source inversion of *W* phase: Speeding up seismic tsunami warning." *Geophysical Journal International* 175, no. 1: 222–38.

Knopoff, Leon, and Freeman Gilbert. 1959. "Radiation from a strike-slip fault." *Bulletin of the Seismological Society of America* 49, no. 2: 163–78.

Martin, Stacey S., Linlin Li, Emile A. Okal, Julie Morin, Alexander E. G. Tetteroo, Adam D. Switzer, and Kerry E. Sieh. 2019. "Reassessment of the 1907 Sumatra 'tsunami earthquake' based on macroseismic, seismological, and tsunami observations and modeling." *Pure and Applied Geophysics* 176, no. 7: 2831–68.

McNamara, Daniel E., and Raymond P. Buland. 2004. "Ambient noise levels in the continental United States." *Bulletin of the Seismological Society of America* 94, no. 4: 1517–27.

Meinig, Christian, Scott E. Stalin, Alex I. Nakamura, Frank González, and Hugh B. Milburn. 2005. "Technology developments in real-time tsunami measuring, monitoring and forecasting." In *Proceedings of OCEANS 2005 MTS/IEEE*, pp. 1673–79. IEEE.

Mendiguren, Jorge A. 1971. "Focal mechanism of a shock in the middle of the Nazca plate." *Journal of Geophysical Research* 76, no. 17: 3861–79.

Mungov, George, Marie Eblé, and Richard Bouchard. 2013. "DART® tsunameter retrospective and real-time data: A reflection on 10 years of processing in support of tsunami research and operations." *Pure and Applied Geophysics* 170, no. 9–10: 1369–84.

Natawidjaja, Danny H., Kerry Sieh, Mohamed Chlieh, John Galetzka, Bambang W. Suwargadi, Hai Cheng, R. Lawrence Edwards, Jean-Philippe Avouac, and Steven N. Ward. 2006. "Source parameters of the great Sumatran megathrust earthquakes of 1797 and 1833 inferred from coral microatolls." *Journal of Geophysical Research: Solid Earth* 111, no. B6: B06403, 37 pp.

Newman, Andrew V., Gavin Hayes, Yong Wei, and Jaime Convers. 2011. "The 25 October 2010 Mentawai tsunami earthquake, from real-time discriminants, finite-fault rupture, and tsunami excitation." *Geophysical Research Letters* 38, no. 5: L05302, 7 pp.

Newman, Andrew V., and Emile A. Okal. 1998. "Teleseismic estimates of radiated seismic energy: The E/M_0 discriminant for tsunami earthquakes." *Journal of Geophysical Research: Solid Earth* 103, no. B11: 26885–98.

Okal, E. A. 1992. Use of the mantle magnitude M_m for the reassessment of the moment of historical earthquakes." *Pure and Applied Geophysics (PAGEOPH)* 139: 17–57. https://doi.org/10.1007/BF00876825.

Okal, Emile A. 2013. "From 3-Hz *P* waves to ${}_0S_2$: No evidence of a slow component to the source of the 2011 Tohoku earthquake." *Pure and Applied Geophysics* 170, no. 6–8: 963–73.

Okal, Emile A. 2019. "Energy and magnitude: a historical perspective." *Pure and Applied Geophysics* 176, no. 9: 3815–49.

Okal, Emile A., and José C. Borrero. 2011. "The 'tsunami earthquake' of 1932 June 22 in Manzanillo, Mexico: Seismological study and tsunami simulations." *Geophysical Journal International* 187, no. 3: 1443–59.

Okal, Emile A., and Jacques Talandier. 1989. "M_m: A variable-period mantle magnitude." *Journal of Geophysical Research: Solid Earth* 94, no. B4: 4169–93.

Okal, Emile A., and Jacques Talandier. 1997. "*T* waves from the great 1994 Bolivian deep earthquake in relation to channeling of *S* wave energy up the slab." *Journal of Geophysical Research: Solid Earth* 102, no. B12: 27421–37.

Paros, J., P. Migliacio, T. Schaad, W. Chadwick, C. Meinig, M. Spillane, L. Tang, and S. Stalin. 2012. "Nano-resolution technology demonstrates promise for improved local tsunami warnings on the MARS project." In *2012 Oceans-Yeosu*, pp. 1–6. IEEE.

Polet, Jascha, and Hiroo Kanamori. 2000. "Shallow subduction zone earthquakes and their tsunamigenic potential." *Geophysical Journal International* 142, no. 3: 684–702.

Richter, Charles F. 1935. "An instrumental earthquake magnitude scale." *Bulletin of the Seismological Society of America* 25, no. 1: 1–32.

Salaree, Amir, and Emile A. Okal. 2018. "The 'tsunami earthquake' of 13 April 1923 in Northern Kamchatka: Seismological and hydrodynamic investigations." *Pure and Applied Geophysics* 175, no. 4: 1257–85.

Saloor, Nooshin, and Emile A. Okal. 2018. "Extension of the energy-to-moment parameter Θ to intermediate and deep earthquakes." *Physics of the Earth and Planetary Interiors* 274: 37–48.

Sella, Giovanni F., Timothy H. Dixon, and Ailin Mao. 2002. "REVEL: A model for recent plate velocities from space geodesy." *Journal of Geophysical Research: Solid Earth* 107, no. B4: ETG-11, 32 pp.

Stein, Seth, and Michael Wysession. 1991. *An Introduction to Seismology, Earthquakes, and Earth Structure.* Blackwell.

Synolakis, Costas, Emile Okal, and Eddie Bernard. 2005. "The mega-tsunami of December 26, 2004." *Bridge*, 35, no. 2: 26–35.

Tanioka, Yuichiro, Larry Ruff, and Kenji Satake. 1997. "What controls the lateral variation of large earthquake occurrence along the Japan Trench?" *Island Arc*, 6, no. 3: 261–66.

Teng, Chung-Chu, Stephen Cucullu, Shannon McArthur, Craig Kohler, Bill Burnett, and Landry Bernard. 2010. *Buoy Vandalism Experienced by NOAA National Data Buoy Center.* National Oceanic and Atmospheric Administration Stennis Space Center MS National Data Buoy Center, 10 pp.

Vaněk, Jiří, Alois Zátopek, Vit Kárník, Natalya V. Kondorskaya, Yuriĭ V. Riznichenko, Evgeniĭ F. Savarenskiĭ, Sergeĭ L. Solov'ev, and Nikolaĭ V. Shebalin, 1962. Standardizatsya shkaly magni-

tud, *Izv. Akad. Nauk SSSR, Ser. Geofiz.*, 2, 153–158, 1962 [in Russian]; English translation, *Bull. USSR Acad. Sci.*, 2:108–11.

Vvedenskaya, A. V. 1956. "Opredelenie poleí smeshcheni pri zemletryaseniyakh s pomoshchyu teori dislokatsiĭ." *Izv. Akad. Nauk SSSR, Ser. Geofiz.* 3: 277–84.

Wessel, Paul, and Walter H. F. Smith. 1991. "Free software helps map and display data." *EOS, Transactions American Geophysical Union* 72, no. 41: 441, 445–46.

Zachariasen, Judith, Kerry Sieh, Frederick W. Taylor, R. Lawrence Edwards, and Wahyoe S. Hantoro. 1999. "Submergence and uplift associated with the giant 1833 Sumatran subduction earthquake: Evidence from coral microatolls." *Journal of Geophysical Research: Solid Earth* 104, no. B1: 895–919.